# Effects of Process Variables and Size Scale on Solidification Microstructure in Laser-Based Solid Freeform Fabrication of Ti-6Al-4V

**N.W. Klingbeil, S. Bontha, C.J. Brown and D.R. Gaddam**
Department of Mechanical and Materials Engineering
Wright State University
Dayton, OH 45435

**P.A. Kobryn**
Materials and Manufacturing Directorate (AFRL/MLSC)
Air Force Research Laboratory
WPAFB, OH 45433

**H.L. Fraser**
Department of Materials Science and Engineering
The Ohio State University
Columbus, OH 43210

**J.W. Sears**
Additive Manufacturing Laboratory
South Dakota School of Mines and Technology
Rapid City, SD 57701

**Abstract:**

This paper summarizes a combination of analytical and numerical modeling approaches which have been used to investigate the effects of process variables and size scale on solidification microstructure in laser-deposited Ti-6Al-4V. The analytical approach is based on the well-known Rosenthal solution for a moving point heat source, which provides dimensionless process maps for solidification cooling rate and thermal gradient (the key parameters controlling microstructure) as a function of laser deposition process variables (laser power and velocity). Based on these process maps, results for both 2-D thin-wall and bulky 3-D geometries are plotted on solidification maps for predicting grain morphology in laser-deposited Ti-6Al-4V. Although the Rosenthal results neglect the nonlinear effects of temperature-dependent material properties and latent heat of transformation, a comparison with 2-D and 3-D nonlinear thermal finite element results for both small-scale (LENS$^{TM}$) and large-scale (high power) processes suggests that they can provide reasonable estimates of trends in grain morphology. Finally, 3-D cellular automaton solidification modeling is used to provide direct predictions of solidification microstructure, and results are compared to experimental observations for both LENS$^{TM}$ and a larger scale process under development at SDSM&T. The results of this work suggest that changes in process variables could potentially result in a grading of the microstructure throughout the depth of the deposit, and that a transition from columnar to equiaxed microstructure is possible at high laser powers.

## Introduction

This work is part of a broader effort to tackle the primary obstacles to the widespread commercialization of laser-based additive manufacturing processes, which include the control of melt pool size, residual stress and microstructure [1]. The current study focuses on the prediction of trends in solidification microstructure, with specific application to Ti-6Al-4V.

Laser-based additive manufacturing of Ti-6Al-4V is currently under consideration for application to aerospace components, for which consistent microstructure and resulting mechanical properties are of vital importance [2,3]. However, only limited experimental data exists to link deposition process variables (e.g., laser power and velocity) to resulting microstructure (e.g., grain size and morphology) [4-8], and suitable microstructures have typically been obtained only by trial and error. In addition, it is unclear whether knowledge based on small-scale laser deposition processes (e.g., LENS$^{TM}$) can be applied to large-scale (higher power) processes currently under development for commercial application.

The current study employs a combination of analytical and numerical modeling approaches to investigate the effects of process variables and size scale on solidification microstructure in laser-deposited Ti-6Al-4V. The analytical approach is based on the well-known Rosenthal solution for a moving point heat source traversing an infinite substrate [9], which has been used recently in the literature to guide the development of process maps relating laser deposition process variables to melt pool size and residual stress [10-13]. Based on the Rosenthal solution, thermal process maps for solidification cooling rate and thermal gradient (the key parameters controlling microstructure) have been presented in [14], and are used herein to provide general insights into the roles of process variables and size scale on microstructure in laser deposited materials.

While the Rosenthal solution assumes temperature-independent material response, the nonlinear effects of temperature-dependent properties and latent heat are further included through thermal finite element modeling. Continuum finite element modeling of laser deposition processes is well established, and has been successfully used to study the effects of process variables on melt pool size and residual stress [10-13]. In the current study, the primary purpose of the finite element modeling is to assess the validity of the Rosenthal results for predicting trends in solidification microstructure. This has been investigated for small-scale (LENS$^{TM}$) deposition of thin-wall geometries in [14-15], and is extended herein to include 3-D finite element modeling of bulky 3-D geometries for both small-scale (LENS$^{TM}$) and large-scale (higher power) processes. Numerical results extracted from both the Rosenthal and FEM solutions are plotted on solidification maps for predicting grain morphology in Ti-6Al-4V, and the utility of the Rosenthal solution is discussed.

Finally, 3-D cellular automaton modeling is used to provide direct predictions of solidification microstructure in laser-deposited Ti-6Al-4V. Cellular automaton modeling originally developed for casting processes [16] has been recently applied to laser deposition of both titanium and aluminum alloys [15,17], and shows strong potential for linking process variables with microstructure in laser materials processing. In this study, results obtained for a thin-wall geometry are compared to experimental observations for the LENS$^{TM}$ process, while results for a bulky 3-D geometry are compared to experimental observations for a somewhat larger scale process under development at the South Dakota School of Mines and Technology (SDSM&T).

The results of this work suggest that size scale can potentially have a significant effect on microstructure, including a transition from columnar to equiaxed microstructure at high laser powers. These results are particularly relevant in light of recent investigations into the effects of process scaling on the control of melt pool size in laser-based manufacturing processes [18,19].

**Geometries Considered**

The modeling described herein considers both the thin-wall (2-D) and bulky (3-D) geometries of Figure 1, in which the process variables of interest are the absorbed laser power $\alpha Q$ and velocity $V$. In each case, it is assumed that the height $h$ and length $L$ are sufficiently large such that the steady-state Rosenthal solution for a point heat source traversing an infinite half-space applies [9]. In the current study, the geometry of Fig. 1a is used to investigate small-scale deposition of thin-wall structures, such as those commonly manufactured using the LENS$^{TM}$ process. The geometry of Fig. 1b is used to investigate both small-scale and large-scale (high power) deposition of bulky 3-D deposits, and provides significant insight into the effect of process size scale on solidification microstructure.

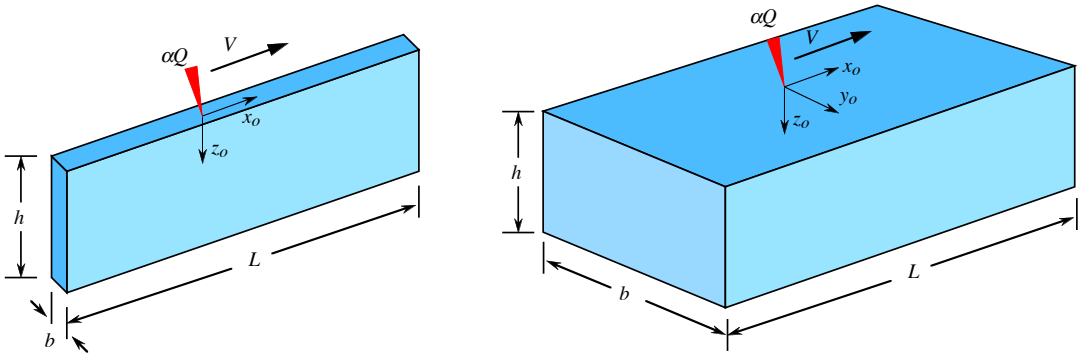


Figure 1. a) Thin-Wall (2-D) and b) Bulky (3-D) Geometries Considered

**Rosenthal Solution and Thermal Process Maps**

Thermal process maps for solidification cooling rate and thermal gradient (the key parameters controlling microstructure) have been developed based on the Rosenthal solution for a moving point heat source traversing an infinite substrate [9]. The details of this development are outlined in [14], and are only briefly summarized here.

*Process Maps for Thin-Wall Geometries*

As described in [14], the dimensionless solidification cooling rate and thermal gradient for the thin-wall geometry of Fig. 1a can be numerically extracted from the 2-D Rosenthal solution, and take the form

$$\frac{\partial \bar{T}}{\partial \bar{t}} = \left(\frac{2\pi k^2 b}{\alpha Q \rho c V^2}\right)\frac{\partial T}{\partial t}, \quad \left|\overline{\nabla T}\right| = \left(\frac{2\pi k^2 b}{\alpha Q \rho c V}\right)\left|\nabla T\right|. \tag{1}$$

The results are plotted in Figure 2 as a function of normalized melting temperature $\bar{T}_m$ and relative depth within the melt pool $\bar{z}_o/\bar{z}_m$. The normalized melting temperature varies with laser power, and is defined as

$$\bar{T}_m = \frac{T_m - T_o}{\alpha Q / \pi k b}. \tag{2}$$

In the above equations, $T_m$ is the melting temperature of the material, $T_o$ is the initial temperature of the wall, $b$ is the wall thickness, and $\rho$, $c$ and $k$ are the density, specific heat and thermal conductivity of the material, respectively. The normalized depth varies in the range $0 \le \bar{z}_o/\bar{z}_m \le 1$, where $\bar{z}_m$ signifies the deepest extent of the melt pool for a given value of $\bar{T}_m$.

The results of Fig. 2 indicate that for a fixed laser velocity, changes in laser power (or changes in $\overline{T}_m$) can have a significant effect on the solidification cooling rate and thermal gradient, and hence the resulting microstructure. For a given laser power and velocity, the cooling rate varies significantly throughout the depth of the melt pool, while the thermal gradient is insensitive to depth. Moreover, increasing laser power (or decreasing $\overline{T}_m$) results in a substantial decrease in thermal gradient throughout the depth of the melt pool, while the cooling rate is most significantly affected at the surface. Hence, increasing laser power (i.e., increasing process size scale) acts to decrease the high thermal gradients typically associated with a columnar microstructure, with an increase in solidification rates toward the surface of the deposit. This suggests the potential for a grading of the microstructure throughout the depth of the deposit, with a transition from columnar to equiaxed microstructure at the surface.

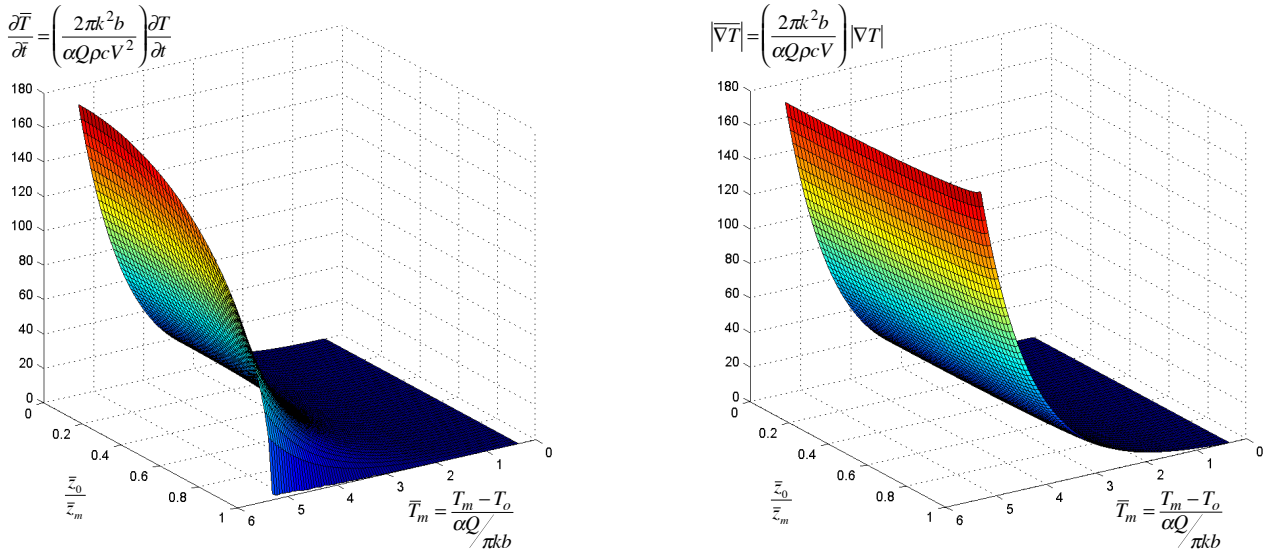


a) b)

Figure 2. Process Maps for Solidification a) Cooling Rate and b) Thermal Gradient for Thin-Wall Geometries [14]

Changes in laser velocity further affect cooling rate and thermal gradient through the normalizations of eq. (1), which reveal that cooling rate is the more sensitive of the two. However, both the thermal gradient and solidification velocity (the ratio of cooling rate to thermal gradient) scale linearly with laser velocity, which depending on the material system can also influence trends in grain morphology. That said, the laser velocities used in small-scale and large-scale processes can be comparable (on the order of 10-20 *mm/s*), while the range of laser powers can span as much as two orders of magnitude (300-30,000 *W*). As such, the remaining discussions on the effects of process scaling will focus primarily on laser power.

*Process Maps for Bulky 3-D Geometries*

As outlined in [14], the dimensionless solidification cooling rate and thermal gradient for the geometry of Fig. 1b can be numerically extracted from the 3-D Rosenthal solution, and take the form

$$\frac{\partial \overline{T}}{\partial \overline{t}} = \left(\frac{2k}{\rho cV}\right)^2 \left(\frac{\pi k}{\alpha QV}\right) \frac{\partial T}{\partial t}, \quad \left|\overline{\nabla T}\right| = \left(\frac{2k}{\rho cV}\right)^2 \left(\frac{\pi k}{\alpha Q}\right) |\nabla T|. \tag{3}$$

The results are plotted in Figure 3 as a function of normalized melting temperature $\overline{T}_m$ and relative depth within the melt pool $\bar{z}_o / \bar{z}_m$. The dimensionless melting temperature for bulky 3-D geometries is defined herein in terms of both laser power and velocity as

$$\overline{T}_m = \frac{T_m - T_o}{\left(\alpha Q / \pi k\right)\left(\rho cV / 2k\right)}. \tag{4}$$

It should be noted that the above definition of $\overline{T}_m$ is in keeping with that used for bulky 3-D geometries in [14], and differs by a factor of 2 from the definition used by other researchers [18, 20]. It should finally be noted that the presence of the laser velocity $V$ in the temperature normalization of eq. (4) results in a higher order velocity dependence of the cooling rates and thermal gradients of eq. (3), as compared to the 2-D normalizations of eq. (1).

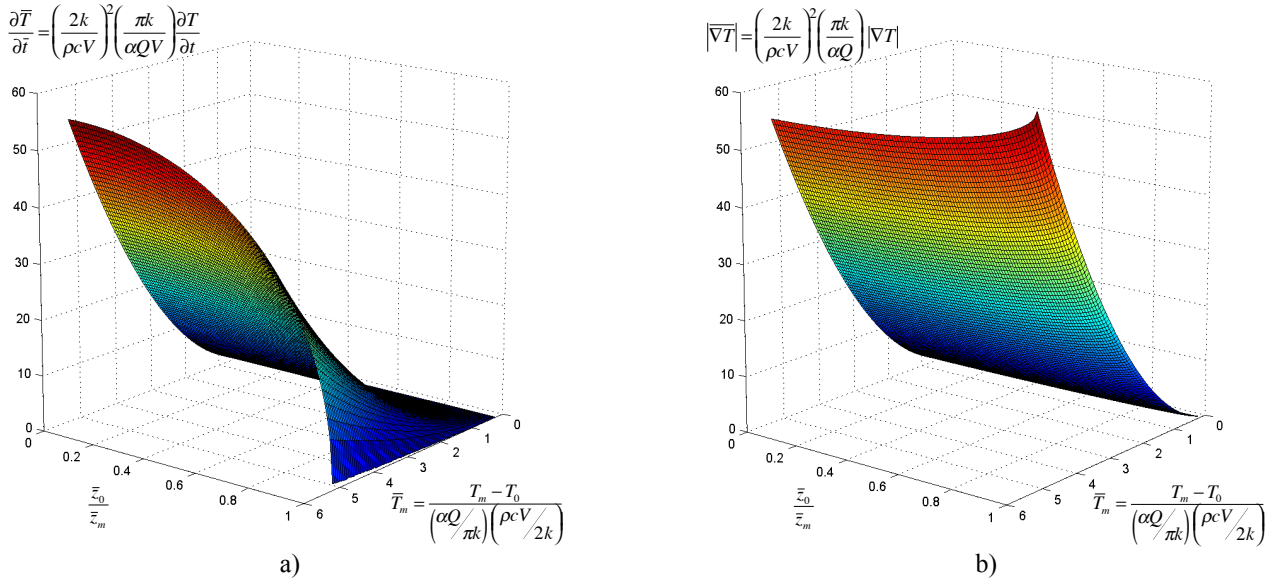


Figure 3. Process Maps for Solidification a) Cooling Rate and b) Thermal Gradient for Bulky (3-D) Geometries [14]

The results of Fig. 3 reveal that for fixed laser velocity, trends in dimensionless cooling rate and thermal gradient are similar to those observed for thin-wall geometries in Fig. 2, except that the dimensionless thermal gradient is slightly more sensitive to depth within the deposit. However, owing to the different temperature normalizations in 2-D and 3-D, comparing the magnitudes of the dimensionless results in Figs. 2 and 3 can be misleading. For example, although the magnitudes of the *dimensionless* cooling rates are larger in Fig. 2a than in Fig. 3a, the *actual* cooling rate for a given laser power and velocity is greater in 3-D than in 2-D. In addition, variations in laser velocity for bulky 3-D geometries affect the value of $\overline{T}_m$, which complicates the interpretation of the axes in Fig. 3. However, if it is assumed that the velocity is held constant, all previous conclusions regarding the effect of laser power (i.e., process size scale) on grain morphology are applicable to both 2-D thin-wall and bulky 3-D deposits.

**Thermal Finite Element Modeling**

While the Rosenthal solution assumes temperature-independent material response, the nonlinear effects of temperature-dependent properties and latent heat have been included through thermal finite element modeling. The modeling procedures for the 2-D thin-wall geometry of Fig. 1a are outlined in [15], and have been extended herein to include the bulky 3-D geometry of Fig. 1b. A representative finite element mesh and boundary conditions for a half-symmetric model of a bulky 3-D geometry is shown in Figure 4. The model uses 8-noded bi-linear thermal elements, and has been generated using the software package ABAQUS. The finite element model approximates the laser deposition process as a moving point heat source $\alpha Q$, which is successively applied to adjacent nodes at time intervals corresponding to the laser velocity $V$. The parameter $\alpha$ represents the fraction of the laser power absorbed by the deposit, and has been estimated as 35%. This value gives reasonable agreement with melt pool sizes observed for the LENS$^{TM}$ process [21]. The remaining boundary conditions are insulated ($q = 0$) on the top and all side faces, and a fixed temperature condition on the bottom ($T = 25\ ^{\circ}C$). Finally, the finite element model uses temperature-dependent specific heat, density and thermal conductivity, and includes latent heat effects for Ti-6Al-4V.

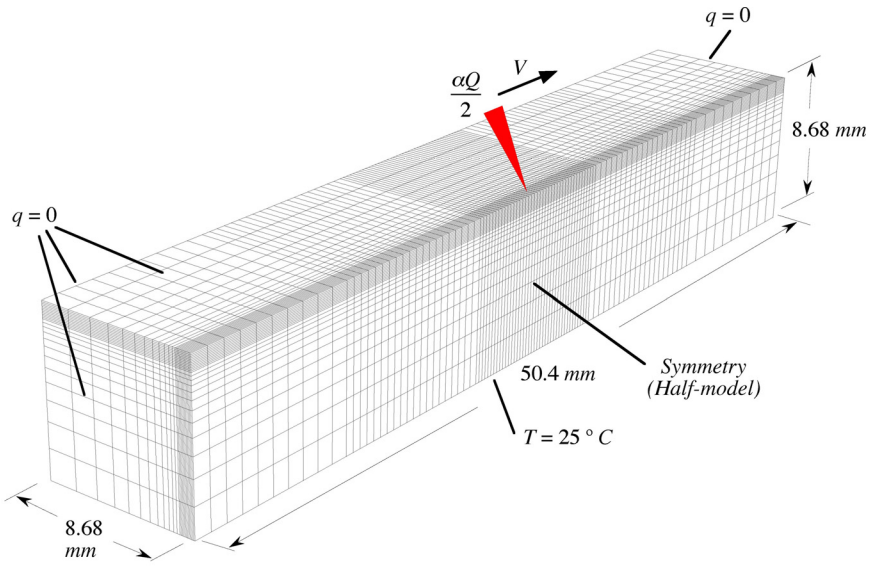


Figure 4. Representative Thermal Finite Element Mesh for the Bulky 3-D Geometry of Figure 1b.

Meshes similar to that of Fig. 4 have been used to investigate both small-scale and large-scale processes, with laser powers ranging from 300-30,000 $W$. In all cases, the mesh dimensions have been scaled to be in keeping with the steady-state Rosenthal solution, so that the behavior in the vicinity of the melt pool is unaffected by the boundaries. In general, the mesh resolution of Fig. 4 has provided more than 10 elements through the depth of the melt pool, from which solidification cooling rates and thermal gradients have been extracted. Procedures for extracting solidification cooling rates and thermal gradients from the finite element results followed those outlined in [15], and are not reiterated here. A rigorous convergence study for the case of temperature-independent properties has recovered solidification cooling rates and thermal gradients within one percent of the Rosenthal results of Fig. 3, which verifies the accuracy of the FEM modeling procedures.

**Solidification Maps for Ti-6Al-4V**

As discussed in [14,15], results for solidification thermal gradient and cooling rate can be interpreted in the context of a solidification map to provide predictions of grain morphology in

laser-deposited Ti-6Al-4V. Given the solidification cooling rate $\partial T/\partial t$ and thermal gradient $G = |\nabla T|$, the solidification velocity $R$ is determined as

$$R = \frac{1}{G}\frac{\partial T}{\partial t}. \tag{5}$$

The expected grain morphology can be predicted as either equiaxed, columnar or mixed by plotting points in $G$ vs. $R$ space (i.e., on the "solidification map"), which has been previously calibrated for Ti-6Al-4V [7].

Solidification maps showing the effect of laser power for small-scale (LENS™) deposition of bulky 3-D geometries are shown in Figure 5. Analogous results for thin-wall geometries are presented in [14]. The results of Fig. 5a are extracted directly from the 3-D Rosenthal results of Fig. 3, with thermophysical properties for Ti-6Al-4V assumed constant at the melting temperature $T_m$=1654°$C$. The results of Fig. 5b are extracted from the thermal finite element model of Fig. 4, with temperature-dependent properties and latent heat effects for Ti-6Al-4V. The range of powers is 350-750 $W$, which is larger than that considered for thin-wall geometries in [14]. In each case, the laser velocity is held constant at $V$ = 8.47 $mm/s$, and the fraction of absorbed laser power is taken to be $\alpha$=0.35.

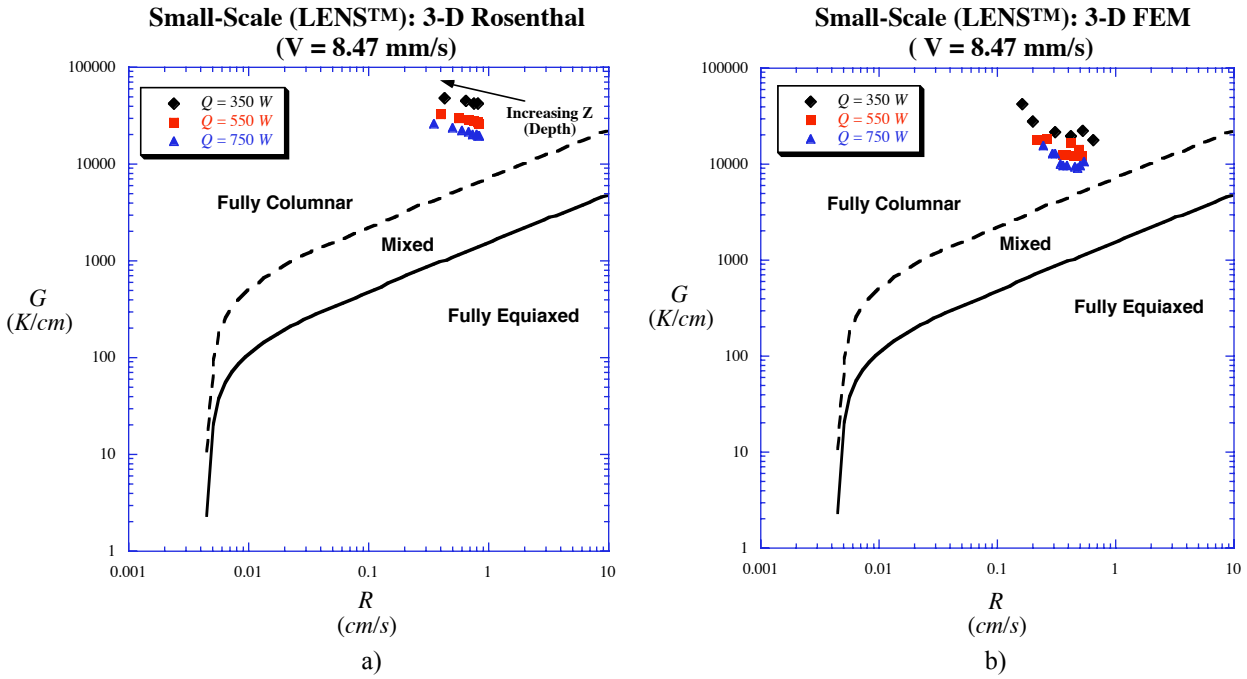


Figure 5. Predicted Ti-6Al-4V Grain Morphology for Small-Scale (LENS™) Deposition of Bulky 3-D Deposits from a) 3-D Rosenthal Solution and b) 3-D FEM

Although the Rosenthal results neglect the nonlinear effects of temperature-dependent properties and latent heat of transformation, trends in $G$ vs. $R$ predictions are in good agreement with those obtained from the FEM results. In particular, both the Rosenthal and FEM results predict a fully columnar morphology, which is in keeping with experimental observations of LENS™ deposited Ti-6Al-4V [5-7]. However, results also suggest that increasing the laser power tends to shift the data closer to the boundary for a mixed columnar/equiaxed grain

morphology. These results are in keeping with $G$ vs. $R$ predictions reported for thin-wall geometries in [14], as well as with experimental observations recently reported in [4].

A comparison of solidification map predictions from the Rosenthal and FEM solutions for large-scale (high power) processes is shown in Figure 6. The range of laser powers considered spans 5-30 $kW$. In each case, the laser velocity is held constant at $V = 8.47$ $mm/s$, and the fraction of absorbed laser power is taken to be $\alpha$=0.35. As observed for small-scale processes, trends in $G$ vs. $R$ predictions from the 3-D Rosenthal and FEM solutions are in good agreement. In particular, both suggest that large-scale processes can result in a grading of the microstructure throughout the depth of the deposit, with a mixed or even fully-equiaxed microstructure at the surface. Moreover, the trend toward equiaxed microstructure increases with laser power.

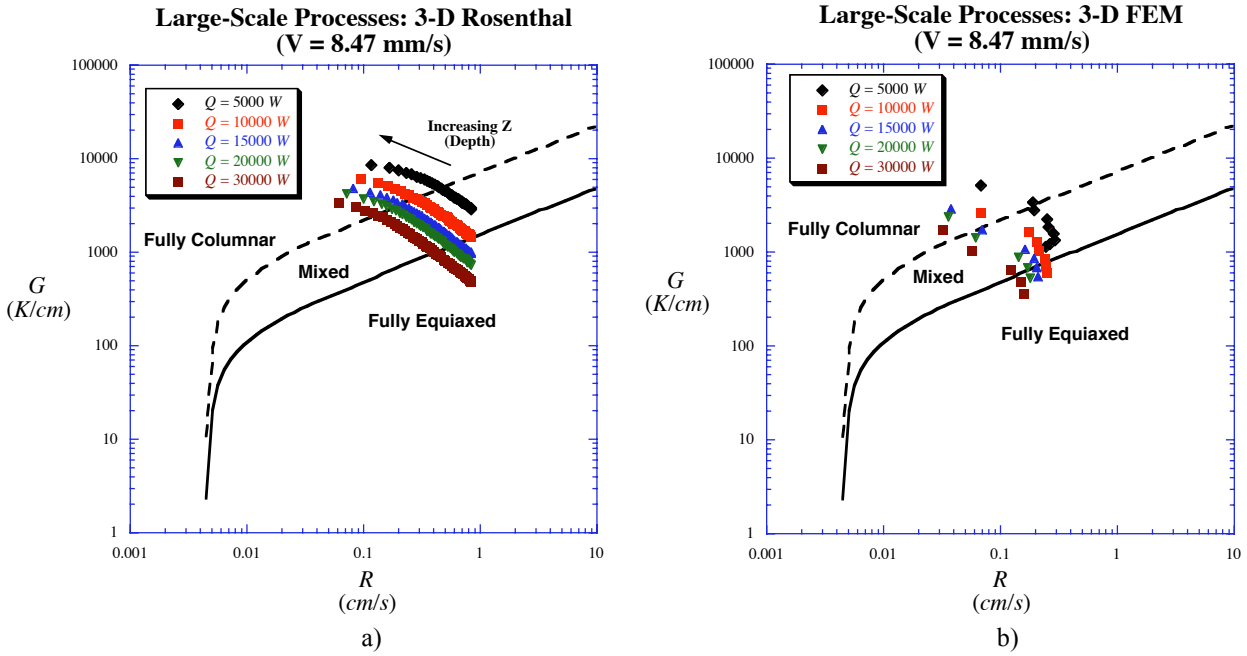


Figure 6. Predicted Grain Morphology for Large-Scale (High-Power) Deposition of Bulky 3-D Deposits from a) 3-D Rosenthal Solution and b) 3-D FEM

The above trends can be inferred from the previous discussion of the thermal process maps of Figs. 2 and 3. In particular, increasing laser power (i.e., size scale) acts to reduce the thermal gradients, which for a fixed cooling rate would move the data down and to the right in $G$ vs. $R$ space. However, increasing power also decreases cooling rates (and hence the solidification rate $R$), which is a competing effect. The net result is an essentially downward movement in $G$ vs. $R$ space. At the same time, cooling rates increase toward the surface of the deposit, and are accompanied by a slight decrease in thermal gradients for bulky 3-D geometries (Fig. 3). This also tends to move the data down and toward the right in $G$ vs. $R$ space. The net result is a trend toward mixed or equiaxed microstructure at the surface, which increases with laser power (i.e., process size scale).

**Cellular Automaton Modeling of Solidification Microstructure**

Cellular automaton (CA) modeling has been used to provide direct predictions of solidification microstructure in laser-deposited Ti-6Al-4V, for both 2-D thin-wall and bulky 3-D geometries. Results for 2-D thin-wall geometries are compared to experimental observations for the LENS™ process, while results for a bulky 3-D geometry are compared to experimental observations for a slightly larger-scale process under development at SDSM&T.

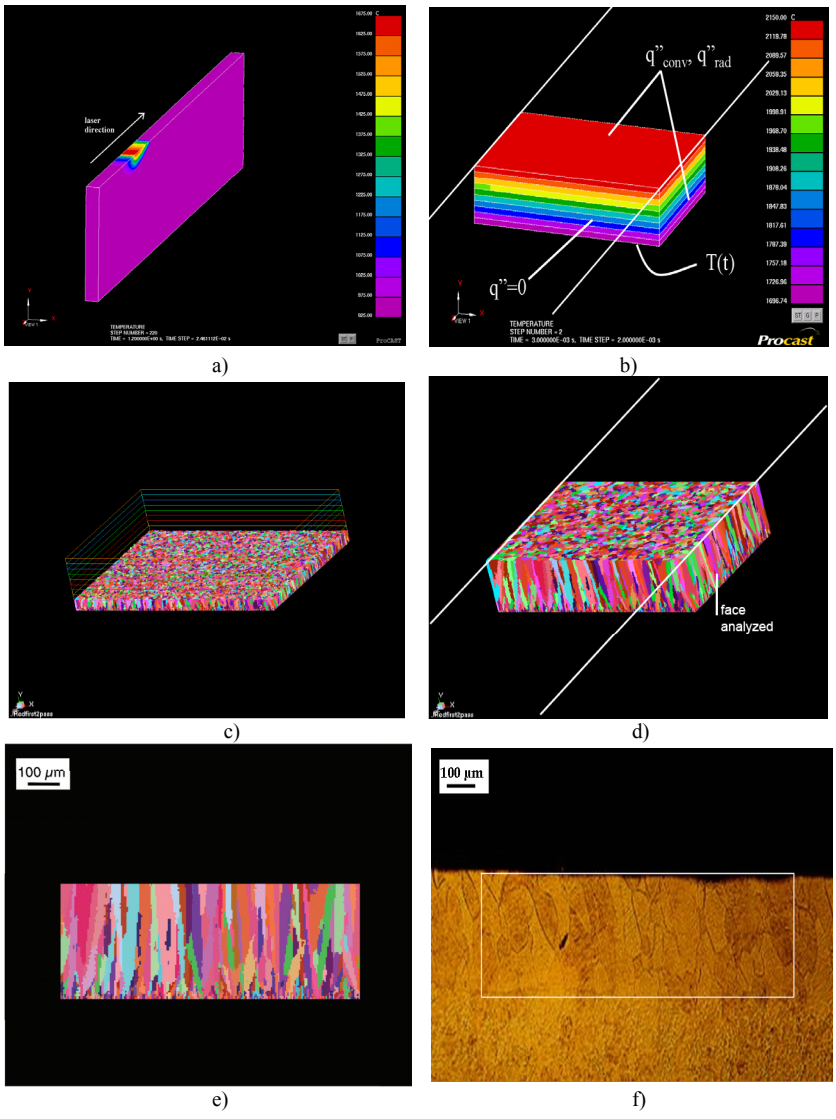


Figure 7. CA Predicted and Observed Microstructures in Thin-Wall LENS™ Deposits ($Q$=370 $W$, $V$=12.5 *mm/s*)

The general procedures used here follow those outlined in [15], and involve 3-D thermal finite element modeling of the laser deposition process using the software package ProCast™, followed by 3-D cellular automaton solidification modeling of grain nucleation and growth using the software package CAFE3D. Detailed background on the algorithms used in CAFE3D can be found in [16]. In brief, the software uses a Gaussian distribution of nucleation sites to simulate the stochastic grain growth process during solidification, and requires statistical solidification parameters for the material system of interest. These parameters, including the mean undercooling, the standard deviation of the undercooling, and the nucleation site density, have been calibrated by direct comparison with bulk solidification of cast Ti-6Al-4V ingots of varying size [21].

*Modeling of Thin-Wall LENS™ Deposits*

Modeling procedures and results for a thin-wall LENS™ geometry are shown in Figure 7. For a given set of process variables (laser power and velocity), thermal history output from a ProCast™ model of the laser deposition process (Fig 7a) is used as input for subsequent CAFE3D cellular automaton analysis of grain nucleation and growth. However, since the CAFE3D software is designed to model solidification from an entirely liquid state, it is necessary

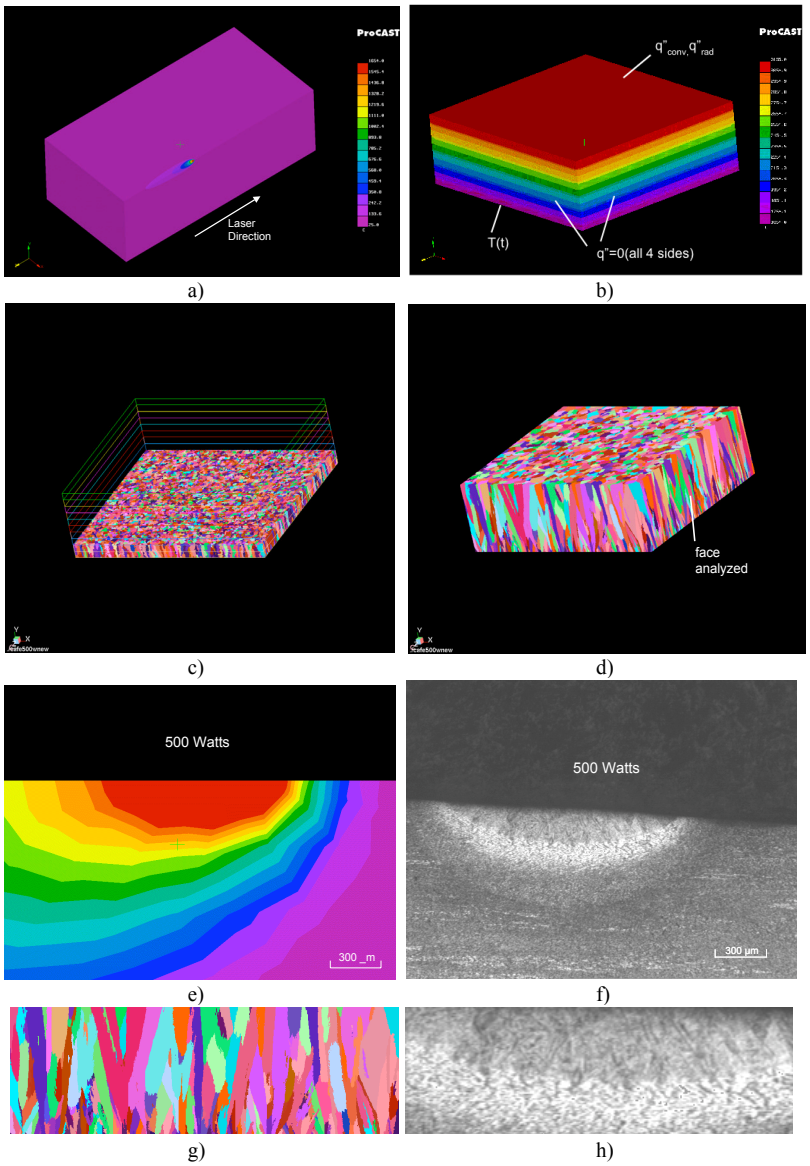


Figure 8. Predicted Microstructure in Bulky 3-D Deposits and Comparison with Laser Glazing at SDSM&T ($Q$=500 $W$, $V$=20 $mm/s$)

to first isolate the melt pool region from the ProCast™ model. As illustrated in Fig. 7b, thermal history data from the section of the model within the melt pool ($T > 1650\ ^{o}C$ ) is extracted from the ProCast™ model, and used to define an equivalent melt pool model suitable for CAFE3D analysis. The initial temperatures and boundary conditions for the melt pool model of Fig. 7b result in largely one-dimensional heat transfer through the depth of the melt pool, which approximates the directional solidification occurring in laser deposition processes.

The evolution of the solidification microstructure is shown in Figs. 7c -d, and a comparison of CAFE3D predictions and observed microstructures for the LENS™ process ($Q$=370 $W$, $V$=12.5 $mm/s$) is shown in Figs. 7e-f. The grain size and morphology of the CAFE3D predictions are in reasonable agreement with the observed microstructure. Both are fully columnar, which is in keeping with solidification map predictions based on both the Rosenthal and 2-D FEM solutions [14,15], as well as previous observations for LENS™ deposition of Ti-6Al-4V [5-7].

*Modeling of Bulky 3-D Geometries*

Similar procedures have been used to model solidification microstructure for bulky 3-D geometries, as shown in Figure 8. Thermal history data from the half-model of Fig. 8a is used to define the equivalent melt pool model of Fig. 8b. Compared to the melt pool model for the 2-D thin-wall geometry, the only difference for the bulky 3-D geometry is the lack of convection and radiation conditions associated with the wall faces. These conditions are replaced by thermal insulation, which results in truly one-dimensional heat conduction through the depth of the melt pool. Evolution of the resulting microstructure for a laser power of 500 W is shown in Figs. 8c-

d. The result is fully columnar, which is in keeping with the solidification map predictions from both the Rosenthal and 3-D FEM results.

Model results are compared to experimental observations for laser glazing experiments conducted at SDSM&T in Figs. 8e-h. This is a somewhat larger-scale process than LENS$^{TM}$, and uses a $CO_2$ laser with powers on the order of 500-1750 *W*. The results of Fig. 8 are for a laser power of 500 *W* and velocity of 20 *mm/s*. The red melt pool region of Fig. 8e assumes an absorbed laser power of $\alpha$=0.35, which gives reasonable agreement with the observed melt pool dimensions of Fig. 8f. A comparison of the predicted and observed microstructures is shown in Figs. 8g-h. Both microstructures are columnar, which is in keeping with the solidification map predictions previously discussed.

To date, the CAFE3D modeling has been successful in predicting the fully columnar microstructures associated with laser deposition at relatively small scales, including both the LENS$^{TM}$ and SDSM&T processes. Similar modeling at higher laser powers is underway, and seeks to confirm the columnar to equiaxed transition predicted by the solidification map approach. It should be noted that there are recent experimental results in the literature to support such a transition, which has been reported for a 14 *kW* large-scale process in [5].

## Summary and Conclusions

This work has employed a variety of analytical and numerical modeling approaches to investigate the effects of process variables and size scale on solidification microstructure in Ti-6Al-4V. Numerical results based on the Rosenthal solution for a moving point heat source have been plotted on solidification maps for predicting grain morphology in laser-deposited Ti-6Al-4V, and are in keeping with results from nonlinear thermal FEM analyses for both small-scale and large-scale (high power) processes. Results suggest that size scale can have a significant effect on grain morphology, with a transition from columnar to mixed/equiaxed microstructure at high powers. Finally, cellular automaton modeling has been used to provide direct predictions of solidification microstructure in both thin-wall and bulky 3-D deposits, and results are in keeping with experimental observations for both the LENS$^{TM}$ and SDSM&T processes.

## Acknowledgements

This work has been supported by the National Science Foundation, grant number DMI-0224517, by the Joint AFRL/DAGSI Research Program, project number ML-WSU-01-11, and by the U.S. Army Research Laboratory and U.S. Army Office under grant number DAAD 19-02-2-001.

## References

1. Beuth, J.L. and Klingbeil, N.W., 2001, "The Role of Process Variables in Laser-Based Direct Metal Solid Freeform Fabrication," *JOM*, Vol. 53, No. 9, pp. 36-39.

2. Kobryn, P.A. and Semiatin, S.L., 2001, "The Laser Additive Manufacture of Ti-6Al-4V," *JOM*, Vol. 53, No. 9, pp. 40-42.

3. Kobryn, P.A. and Semiatin, S.L., 2000, "Laser Forming of Ti-6Al-4V: Research Overview," *Solid Freeform Fabrication Proceedings*, (D.L. Bourell, J.J. Beaman, R.H. Crawford, H.L. Marcus and J.W. Barlow, eds.), Austin, August 2000.

4. Wu, X., Liang, J., Mei, J., Mitchell, C., Goodwin, P.S. and Voice, W., 2004, "Microstructures of Laser-Deposited Ti-6Al-4V," *Materials & Design*, Vol. 25, pp. 137-144.

5. Kobryn, P.A. and Semiatin, S.L., 2003, "Microstructure and Texture Evolution During Solidification Processing of Ti-6Al-4V," *Journal of Materials Processing Technology*, Vol. 135, pp. 330-339.

6. Kobryn, P.A. and Semiatin, S.L., 2001, "Mechanical Properties of Laser-Deposited Ti-6Al-4V," *Solid Freeform Fabrication Proceedings*, (D.L. Bourell, J.J. Beaman, R.H. Crawford, H.L. Marcus and J.W. Barlow, eds.), Austin, August 2001.

7. Kobryn, P.A., Moore, E.H. and Semiatin, S.L., 2000, "The Effect of Laser Power and Traverse Speed on Microstructure, Porosity and Build Height in Laser-Deposited Ti-6Al-4V," *Scripta Materiala,* Vol. 43, pp. 299-305.

8. C. A. Brice, K. I. Schwendner, D. W. Mahaffey, E. H. Moore, and H. L. Fraser, 1999, "Process Variable Effects On Laser Deposited Ti-6Al-4V," *Solid Freeform Fabrication Proceedings*, (D.L. Bourell, J.J. Beaman, R.H. Crawford, H.L. Marcus and J.W. Barlow, eds.), Austin, August 1999.

9. Rosenthal, D., 1946, "The Theory of Moving Sources of Heat and its Application to Metal Treatments," *Transactions of ASME*, Vol. 68, pp. 849-866.

10. Vasinonta, A., Beuth, J.L. and Griffith, M.L.,1999, "Process Maps for Laser Deposition of Thin-Walled Structures," *Solid Freeform Fabrication Proceedings*, (D.L. Bourell, J.J. Beaman, R.H. Crawford, H.L. Marcus and J.W. Barlow, eds.), Austin, August 1999, pp. 383-391.

11. Vasinonta, A., Beuth, J.L. and Griffith, M.L., 2000, "Process Maps for Controlling Residual Stress and Melt Pool Size in Laser-Based SFF Processes," *Solid Freeform Fabrication Proceedings*, (D.L. Bourell, J.J. Beaman, R.H. Crawford, H.L. Marcus and J.W. Barlow, eds.), Austin, August 2000, pp. 200-208.

12. Vasinonta, A., Beuth, J.L. and Griffith, M.L., 2001, "A Process Map for Consistent Build Conditions in the Solid Freeform Fabrication of Thin-Walled Structures," *Journal of Manufacturing Science and Engineering*, Vol. 123, No. 4, pp. 615-622.

13. Vasinonta, A., Beuth, J.L., and Ong, R., 2001, "Melt Pool Size Control in Thin-Walled and Bulky Parts via Process Maps," *Solid Freeform Fabrication Proceedings* (D.L. Bourell, J.J. Beaman, R.H. Crawford, H.L. Marcus, K.L. Wood and J.W. Barlow, eds.), Austin, August 2001, pp. 432-440.

14. Bontha, S. and Klingbeil, N.W., 2003, "Thermal Process Maps for Controlling Microstructure in Laser-Based Solid Freeform Fabrication," *Solid Freeform Fabrication Proceedings*, (D.L. Bourell, R. H. Crawford, J.J. Beaman, K.L. Wood, H.L. Marcus, eds.), Austin, August 2003.

15. Klingbeil, N.W., Brown, C.J., Bontha, S., Kobryn, P.A. and Fraser, H.L., 2002, "Prediction of Microstructure in Laser Deposition of Titanium Alloys," *Solid Freeform Fabrication Proceedings*, (D.L. Bourell, R. H. Crawford, J.J. Beaman, K.L. Wood, H.L. Marcus, eds.), Austin, August 2002, pp. 142-149.

16. Gandin, Ch. A., Desbiolles, J.L., Rappaz, M. and Thevoz, Ph., 1999, "A Three-Dimensional Cellular Automaton-Finite Element Model for the Prediction of Solidification Grain Structures," *Metallurgical and Materials Transactions A*, Vol. 30A, pp. 3153-3165.

17. Grujicic, M. Cao, G. and Figliola, R.S., 2001, "Computer Simulations of the Evolution of Solidification Microstructure in the LENS$^{TM}$ Rapid Fabrication Process," *Applied Surface Science*, Vol. 183, pp. 43-47.

18. Birnbaum, A., Beuth, J.L., and Sears, J.W., 2004, "Scaling Effects in Laser-Based Additive Manufacturing Processes," *Solid Freeform Fabrication Proceedings*, Austin, August 2004 (in the current proceedings).

19. Birnbaum, A., Aggarangsi, P. and Beuth, J., 2003, "Process Scaling and Transient Melt Pool Size Control in Laser-Based Additive Manufacturing Processes," *Solid Freeform Fabrication Proceedings*, (D.L. Bourell, R. H. Crawford, J.J. Beaman, K.L. Wood, H.L. Marcus, eds.), Austin, August 2003.

20. Aggarangsi, P., Beuth, J.L., and Gill, D.D., 2004, "Transient Changes in Melt Pool Size in Laser Additive Manufacturing Processes," *Solid Freeform Fabrication Proceedings*, Austin, August 2004 (in the current proceedings).

21. Brown, C.J., 2003, "Modeling of Solidification Microstructure in Laser-Deposited Ti-6Al-4V," Masters Thesis, Department of Mechanical & Materials Engineering, Wright State University, June 2003.